

Effect of Noise on DNA Sequencing via Transverse Electronic Transport

Matt Krems,[†] Michael Zwolak,^{‡*} Yuriy V. Pershin,[§] and Massimiliano Di Ventra^{†*}

[†]Department of Physics, University of California, San Diego, La Jolla, California; [‡]Theoretical Division, Los Alamos National Laboratory, Los Alamos, New Mexico; and [§]Department of Physics and Astronomy and USC Nanocenter, University of South Carolina, Columbia, South Carolina

ABSTRACT Previous theoretical studies have shown that measuring the transverse current across DNA strands while they translocate through a nanopore or channel may provide a statistically distinguishable signature of the DNA bases, and may thus allow for rapid DNA sequencing. However, fluctuations of the environment, such as ionic and DNA motion, introduce important scattering processes that may affect the viability of this approach to sequencing. To understand this issue, we have analyzed a simple model that captures the role of this complex environment in electronic dephasing and its ability to remove charge carriers from current-carrying states. We find that these effects do not strongly influence the current distributions due to the off-resonant nature of tunneling through the nucleotides—a result we expect to be a common feature of transport in molecular junctions. In particular, only large scattering strengths, as compared to the energetic gap between the molecular states and the Fermi level, significantly alter the form of the current distributions. Since this gap itself is quite large, the current distributions remain protected from this type of noise, further supporting the possibility of using transverse electronic transport measurements for DNA sequencing.

INTRODUCTION

The prospect of sequencing an entire human genome for less than \$1000 (USD) in a matter of hours is becoming closer to reality (1–3). The original DNA-nanopore experiments of Kasianowicz et al. (4) showed polynucleotides can be pulled through nanoscale pores and their translocation detected by measuring the consequent blockage of the ionic current through the pore. Since then, numerous experimental studies have been performed using biological (5–10) and synthetic nanopores (11–16), which probe various physical properties of translocating polynucleotides. This has fueled an enormous amount of research into novel sequencing proposals based on nanopores or nanochannels (1–3).

One sequencing idea suggests detecting transverse electron currents as single-stranded DNA (ssDNA) translocates through a pore (17–20). Previous theoretical work showed the four DNA nucleotides possess statistically distinguishable electronic signatures (17,18) in the form of current distributions when accounting for structural distortions and partial control of the DNA dynamics (i.e., by a transverse field) (18–20). These results indicate DNA sequencing is, in principle, possible via transverse current measurements. However, such studies have neglected scattering processes, such as fluctuations of the environment, which introduce electronic noise, and may thus affect the ability to distinguish the bases.

Recently, experimentalists have successfully embedded electrodes into solid-state nanopores and nanochannels (21–24) and are getting closer to measuring electronic currents with single nucleotides present in the gap between

the electrodes. When the latter is achieved, one question which will arise is how does the noise induced by the environment—noise which is beyond that due to static structural distortions of the nucleotides—affects the nucleotides' electronic signatures, i.e., the current distributions. The environment is composed of ionic and water fluctuations and other excitations that may drastically affect the electron dynamics, and thus the current (25). To complicate matters, the liquid environment can scatter electrons out of their current-carrying states by absorbing them into the solution and allowing the longitudinal field (that pulls the DNA through the pore) to carry them away. The influence of these and related factors can be very important, as seen in previous studies of electronic transport through DNA (26–28), and so far no study has examined such effects in detail.

In this article, we address these issues theoretically. Clearly, a fully time-dependent calculation with inclusion of all these types of scattering processes would be ideal (25). However, the complexity of the problem we consider here, both in the number of atoms involved and the type of scattering processes to take into account, make this type of dynamical calculation unrealistic at present. Instead, we use a simplified model to capture some of the physics we deem important and leave a time-dependent treatment for future investigation.

In general, one expects any type of electronic noise to eventually destroy the capability to distinguish the DNA bases once its strength is sufficiently large. Indeed, we do find this type of behavior. However, the noise strength at which the electronic transport is negatively influenced is very large, beyond the strength one would expect in realistic experimental situations. This is due to the off-resonant nature of tunneling through the nucleotides, and we thus expect this

Submitted March 3, 2009, and accepted for publication June 15, 2009.

*Correspondence: mpzwolak@gmail.com

Editor: Laura Finzi.

© 2009 by the Biophysical Society
0006-3495/09/10/1990/7 \$2.00

doi: 10.1016/j.bpj.2009.06.055

result to be a common feature of molecular junctions. In other words, the separation of the energy levels of the nucleotides from the equilibrium Fermi level protects the electronic signature of the bases. This study will thus help researchers understand future experimental data, and provides further support to the viability of DNA sequencing via transverse electronic transport.

SETUP AND METHODS

As our starting point, we employ molecular dynamics simulations performed with NAMD2 (29) to pull homogeneous ssDNA through a Si_3N_4 nanopore with embedded gold electrodes. Our basic setup is shown in Fig. 1 and is the same as that used in previous work (18,19), except the new trajectories here correspond to longer simulation times. These trajectories give us the real-time atomistic structure of ssDNA as it propagates through the pore. With these structures, we calculate the electronic transport in the transverse direction across the pore. In the latter calculations, we include the effect of noise as discussed below.

The details of the simulations are as follows. The pore is made of 2.4-nm thick silicon nitride material in the β -phase. The nanopore hole has a double-conical shape with a minimum diameter of 1.4 nm located at the center of the membrane and an outer diameter of 2.5 nm (see Fig. 1). The inner diameter is chosen wide enough such that ssDNA is able to pass through but narrow enough that an appreciable tunneling current can be detected. The nanopore is then solvated in a TIP3 water sphere of 6.0-nm radius with spherical boundary conditions in an NVT ensemble and with a 1 M solution of potassium and chlorine ions. The CHARMM27 force field (30,31) is used for the interaction of DNA, water, and ions, whereas UFF (32) parameters are used for the interaction of the Si_3N_4 membrane and other atoms. The Si_3N_4 atoms are assumed to be fixed during the simulation (this does not affect the conclusions). A 1-fs time step is used and the system temperature is kept at room temperature with a Langevin dampening parameter of 0.2 ps^{-1} in

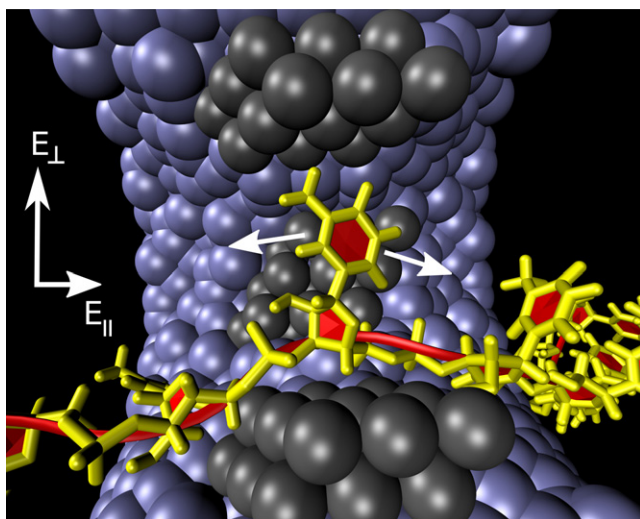


FIGURE 1 Schematic representation of ssDNA translocating through a pore while the transverse electronic current is collected. The light (purple) atoms are the silicon nitride pore and the dark (black) atoms represent the electrode surfaces within our molecular dynamics simulations. The single strand of DNA translocates through the pore pulled by a longitudinal electric field, E_{\parallel} , and the nucleotides also experience a transverse electric field, E_{\perp} . The white arrows around the DNA base indicate an acoustic phononlike motion that contributes to the noise. The visualization was made with VMD (43).

the equations of motion (33). The van der Waals interactions are gradually cut off starting at 10 \AA from the atom until reaching zero interaction 12 \AA away. The energy was initially minimized in 1000 time steps.

A single strand of DNA is constructed by removing one strand from a helical, double-stranded polynucleotide created using the Nucleic Acid Builder of the AmberTools package (34). At the initial time of the simulation, the ssDNA is placed parallel to the pore axis with the first base just inside the pore. The ssDNA is driven through the pore with a global electric field of $6 \text{ kcal}/(\text{mol \AA e})$ to achieve reasonable simulation times. In the calculation of the electronic transport, the longitudinal pulling field is turned off and a transverse field (of the same magnitude as that driving the current) is turned on at a moment when a base is between the electrodes. This approximates the situation when the transverse field is much larger than the longitudinal field. We envision this as the typical operating regime for a sequencing device as it allows for the suppression of a significant amount of structural distortion (18). The particular time to stop the translocation is chosen by visual inspection. This stopping time is not particularly important because it generally takes approximately hundreds of picoseconds for the transverse field, E_{\perp} , to align the nucleotide with the electrodes (19). Single-stranded DNA differs from double-stranded DNA in that the persistence length of the polynucleotide is much shorter. This, in particular, allows for the base to quickly align with the perpendicular electric field. An example of this is reported in Fig. 2, where poly(C)₁₅ is such that a single C base is aligned parallel to a pair of opposite electrodes. A bias of 1 V oriented perpendicular to the base plane is then turned on. From the figure, and in the 1.5 ns Movie S1 in the Supporting Material, it is clear that, for this particular polynucleotide and initial condition, the base and backbone reorient themselves toward the field within $\sim 800 \text{ ps}$. This is also confirmed by the currents as a function of time across two pairs of perpendicularly placed electrodes. At $t = 0$ the largest current is from the pair of electrodes parallel to the plane of the base, whereas after 800 ps, the largest current is from the opposite pair of electrodes. It is also evident from the figure that the rotation does not occur uniformly in time but it proceeds by fast rotations, followed by periods of time in which the system is temporarily trapped in a local energy minimum. Faster rotations have been observed with other initial conditions, transverse voltages, and nucleotide strands (19), but we cannot

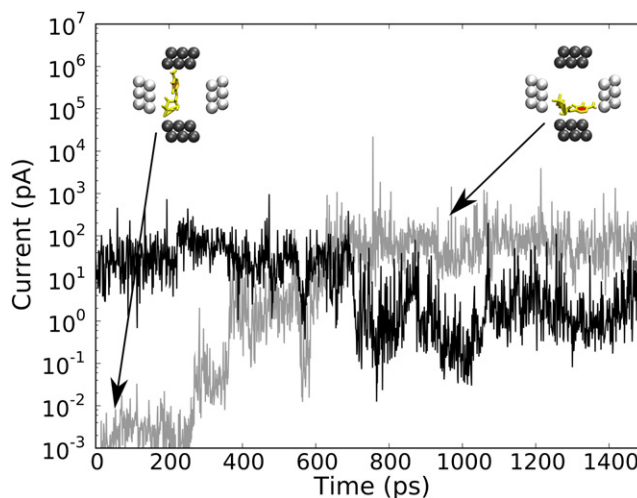


FIGURE 2 Currents as a function of time across two pairs of perpendicularly placed electrodes for poly(C)₁₅ with one base originally aligned parallel to a pair of opposite electrodes (see inset). The black current trace corresponds to the current from the black electrodes, and likewise the gray current trace corresponds to the gray electrodes. At time $t = 0$, a bias of 1 V oriented perpendicular to the base plane is switched on. The corresponding field aligns the base and backbone with the gray pair of electrodes (as shown in the inset), with a corresponding increase in the current across that pair of electrodes.

exclude the possibility that, for other initial conditions, longer times would be needed for a complete rotation of the bases.

The current calculations are performed within a single-particle scattering approach using a tight-binding Hamiltonian (see, e.g., (25)). These calculations include water, although, within our approach, water has little direct effect on the current distributions (19). Snapshots of the atomistic structure of ssDNA between the gold electrodes are taken from the molecular dynamics at regular time intervals. These coordinate snapshots are used to obtain the tight-binding Hamiltonian. For each carbon, nitrogen, oxygen, and phosphorous atom, s , p_x , p_y , and p_z orbitals are used, whereas for gold and hydrogen, only s orbitals are employed. The Fermi level is taken to be that of bulk gold. (The tight-binding Hamiltonian is constructed at every snapshot using the YAEHMOP package, found at <http://yaehmop.sourceforge.net/>. The Fermi level of bulk gold is also calculated using this method.)

To obtain the current across the ssDNA, we use the retarded Green's function,

$$G_{\text{DNA}}(E) = \frac{1}{ES_{\text{DNA}} - H_{\text{DNA}} - \Sigma_t - \Sigma_b - \Sigma_n}, \quad (1)$$

where E is the energy, S_{DNA} and H_{DNA} are the overlap and Hamiltonian matrices, respectively, of the contents of the gap between the electrodes (we will call it electronic junction), $\Sigma_{t(b)}$ terms are the self-energy terms associated with the interaction between the electrodes and the junction contents, and Σ_n is the self-energy associated with the noise. The Green's function for gold needed to calculate $\Sigma_{t(b)}$ is approximated as in Pecchia et al. (35). We use a white-noise term, which corresponds to a noise timescale via

$$\tau_n = -\frac{\hbar}{\text{Im}\{\Sigma_n\}}, \quad (2)$$

and we also take $\text{Re}\{\Sigma_n\} = 0$ (see **Results and Discussion**). This timescale sets a decay time due to interaction with the environment. The latter can be thought of as a noise probe that interacts with the contents of the junction (25,36).

If we were to follow this type of reasoning we would then set the current in the probe to be zero and calculate the total transmission coefficient as

$$T(E) = T_{\text{tb}}(E) + T_{\text{p}}(E), \quad (3)$$

where

$$T_{\text{tb}}(E) = \text{Tr}[\Gamma_t G_{\text{DNA}} \Gamma_b G_{\text{DNA}}^\dagger] \quad (4)$$

is the transmission coefficient that directly couples electrodes that measure the current in the presence of the noise probe with $\Gamma_{t(b)} = i(\Sigma_{t(b)} - \Sigma_{t(b)}^\dagger)$. This transmission contribution includes only elastic processes, as we discuss in more detail below.

The other term is

$$T_{\text{p}}(E) = \frac{T_{\text{tn}} T_{\text{nb}}}{T_{\text{tn}} + T_{\text{nb}}}, \quad (5)$$

where

$$T_{\mu\nu}(E) = \text{Tr}[\Gamma_\mu G_{\text{DNA}} \Gamma_\nu G_{\text{DNA}}^\dagger] \quad (6)$$

is instead the transmission from reservoir μ to ν , namely it takes into account processes that can drive electrons out of the electrodes into the noise probe and vice versa.

The current is then given by

$$I = \frac{2e}{h} \int_{-\infty}^{\infty} dE T(E) [f_t(E) - f_b(E)], \quad (7)$$

where $f_{t(b)}$ is the Fermi-Dirac function of the top (bottom) electrode (25). The current distribution for a nucleotide is the distribution obtained from the various snapshots while the nucleotide fluctuates between the electrodes.

We will later make a microscopic connection to the above transmission probability by starting with a Hamiltonian for independent electrons coherently coupled to a phonon environment. However, this analysis leads us to conclude that in the complex liquid environment, the term in Eq. 5 cannot correctly represent the physical situation at hand. In fact, retention of such term would give rise to unrealistically large currents (several orders-of-magnitude larger than what we present here). Although this result would naively suggest that such currents could in fact be observed in our case, it is unlikely that the nanopore environment would allow for the coherent coupling between the electrons and excitations that gives this increased current. Furthermore, it is likely that due to the presence of the longitudinal field that drives the DNA through the pore the electrons scatter out of their current-carrying states. In this work we will then assume that current-carrying electrons can be scattered into the complex liquid environment and retain only the first term T_{tb} in the transmission probability of Eq. 3, and analyze its effect as a function of the timescale strength τ_n . This is equivalent to assuming that the liquid environment is represented by two probes connected to the junction, and the probes' electrochemical potentials are adjusted so that the combined current from the two probes into either electrode is zero. This condition entails that $I_1 + I_2 = 0$, where 1 and 2 are the two probes. This, together with current conservation, $I_t + I_b + I_1 + I_2 = 0$, yields $I_t = -I_b$, which is the current calculated in this article.

Noise

As stated above, previous theoretical studies have shown the current distributions caused by DNA static structural distortions are statistically distinguishable (17–20). These studies, however, have not included the effects of external noise. We focus specifically on noise given by Eq. 2 because it represents many processes that happen in an experiment. These include fast processes, such as electronic interactions with bound waters or charges on the pore walls, and also slow processes, such as the dynamic movement of the DNA bases and ions. From visual inspection of the molecular dynamics simulations, we observe that the bases fluctuate in a way reminiscent of acoustic phonons, i.e., we observe only low-energy excitations. An example of these excitations is represented in Fig. 1 where these slow oscillations, although not periodic, are mostly in the longitudinal direction. No oscillations where the bases are, e.g., in a breathing mode—where the base itself is expanding and contracting, causing large energy relaxation—were observed. At low bias, these are also unlikely to be excited by the electrical current itself, so that we expect a low exchange of energy with the current-carrying electrons (37,38). Furthermore, we assume the timescale for noise, Eq. 2, is a constant for all molecular states in the junction. In certain cases, this most likely overestimates the effect of the noise, but, on the other hand, it misses colored-noise effects, where, for instance, the noise has a strong component at a particular frequency. In the absence of a physical model for such noise which is supported by experiments, its effect is only speculative at this stage, and we thus defer its study for future research.

RESULTS AND DISCUSSION

We have performed current calculations for some representative noise timescales (39): $\tau_n = \infty$, 10^{-13} , 10^{-14} , 10^{-15} , and 10^{-16} s with transverse voltages of 0.1 V and 1.0 V. The timescale of 10^{-16} s is a particularly fast and unphysical timescale, but was used to show the onset of major differences in the current and current distributions.

For weak noise, ($\tau_n = 10^{-13}$ s– 10^{-14} s), the average current itself is essentially unchanged as well as the distributions. The average percent change of an individual current value for $\tau_n = 10^{-13}$ s is only $\sim 0.1\%$. For $\tau_n = 10^{-14}$ s, it is 1.5%. However, for a single current count, the current may vary by orders

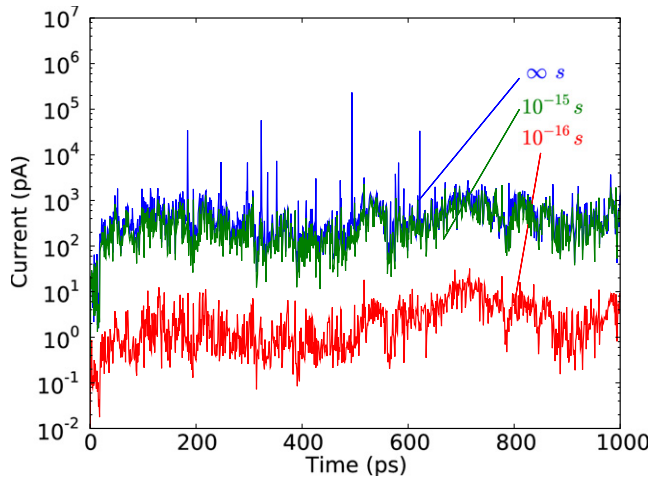


FIGURE 3 Transverse current versus time for poly(A)₁₅ at a transverse bias voltage of 1.0 V. The noise lowers the current slightly for $\tau_n = 10^{-15}$ s. Only at the unrealistic $\tau_n = 10^{-16}$ s does the current shift significantly. Slower noise timescales give essentially the same current as the case with an infinite noise timescale.

of magnitude due to the noise, further strengthening the argument that a single base measurement is likely not enough to distinguish the bases (18). From Figs. 3 and 4, $\tau_n = 10^{-15}$ s lowers the current on average and slightly alters the distributions. There is an average current reduction of $\sim 30\%$. At the unphysical fast timescale of 10^{-16} s, the current is significantly lowered and the distributions are pushed into an unmeasurable regime. However, we are not aware of a physical process that may cause such strong noise under the experimental conditions envisioned in this work.

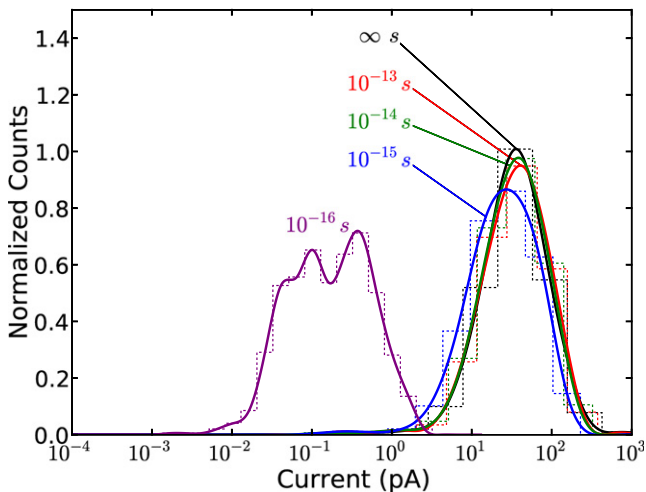


FIGURE 4 Probability distributions for poly(A)₁₅ with various noise timescales for a transverse bias voltage of 1.0 V. The very light dashed lines correspond to the bins used to produce the current distributions. The solid lines are interpolated from the dashed ones. Like the current itself, only with very fast noise, $\tau_n = 10^{-16}$ s, does the distribution change and shift appreciably. At $\tau_n = 10^{-15}$ s, the distribution's mean shifts slightly and it broadens somewhat.

We have found above that even relatively strong noise does not negatively affect the current distributions. This may seem an unexpected result, and it will be helpful for future experimental and theoretical efforts to understand the reason for such an effect. We thus develop a model system to understand this behavior, as well as the noise processes we are including. Our starting point is based on our previous work on transverse transport through DNA (17–20). In an ideal configuration of a nucleotide between electrodes, the LUMO level of the base is closest to the gold Fermi level (1,17) and also couples well to both electrodes. Thus, it is reasonable to treat a nucleotide in the electronic junction as a single energy level, E_0 .

At this point we may consider a model Hamiltonian representing this level interacting with a bosonic environment (note that, for simplicity, we set $\hbar = 1$ in Eqs. 8–14),

$$H = E_0 d^\dagger d + H_{de} + H_e + d^\dagger d \sum_k g_k (b_k^\dagger + b_k) + \sum_k \omega_k b_k^\dagger b_k, \quad (8)$$

where $d^\dagger d$ represents the occupation of the DNA LUMO level, H_{de} is the DNA-electrode interactions, and H_e is the electrodes' Hamiltonian. The two remaining terms represent an interaction with a bosonic environment in the junction with interaction strength g_k to each mode k . To get a tractable model, we make a few additional assumptions. First, we assume the junction DNA energy level is equally coupled to all levels of both electrodes and that we are at low enough bias and temperature (compared with electronic energies) that the electrodes bandwidth is effectively infinite. Second, we assume that the bosonic environment does not generate electronic correlations in the electrodes, which is reasonable for the small electrode coupling that we have here. Within these approximations, the real-time retarded Green's function, Eq. 1, becomes (40,41)

$$G_{\text{DNA}}(t) = -i\Theta(t)e^{-i\tilde{E}_0 t}e^{-\gamma t}e^{-\phi(t)}. \quad (9)$$

This Green's function includes the coupling to the electrodes through the factor $e^{-\gamma t}$, where γ is the coupling strength to both electrodes, and includes the coupling to the bosons through the factor $e^{-\phi(t)}$ and the renormalized energy \tilde{E}_0 . The bosonic term is

$$\phi(t) = \sum_k \frac{|g_k|^2}{\omega_k^2} [n_k(1 - e^{i\omega_k t}) + (n_k + 1)(1 - e^{-i\omega_k t})], \quad (10)$$

where $n_k = 1/(\exp(\beta\omega_k) - 1)$ is the equilibrium occupation of mode k at inverse temperature β . So long as the temperature is large compared to the boson cutoff frequency, ω_c , then $n_k \approx 1/(\beta\omega_k)$ and $n_k \approx n_k + 1$, thus

$$\phi(t) \approx \sum_k \frac{2|g_k|^2}{\beta\omega_k^3} (1 - \cos \omega_k t). \quad (11)$$

In terms of the spectral function, $J(\omega) = \sum_{\mathbf{k}} |g_{\mathbf{k}}|^2 \delta(\omega - \omega_{\mathbf{k}})$,

$$\phi \approx \int_0^{\omega_c} \frac{2J(\omega)}{\beta\omega^3} (1 - \cos \omega t) d\omega. \quad (12)$$

Similarly, the renormalized energy state is

$$\tilde{E}_0 = E_0 + \int_0^{\omega_c} \frac{J(\omega)}{\omega} d\omega. \quad (13)$$

For an Ohmic boson bath (42), $J(\omega) = \alpha\omega$ for $\omega < \omega_c$. At high temperature with respect to its cutoff frequency, $\phi(t) \approx \eta t$, where $\eta = \alpha\pi/\beta$, and $\tilde{E}_0 = E_0 + \alpha\omega_c$. Generally ω_c is quite small compared to molecular energies; we thus ignore the energy shift, which is valid except when the noise strength is very large. This gives

$$G_{\text{DNA}}(E) = \frac{1}{E - E_0 + i\gamma + i\eta} \quad (14)$$

for the retarded Green's function. In this work, $\eta = \hbar/\tau_n = 0$, 6.6×10^{-3} , 6.6×10^{-2} , 6.6×10^{-1} , and 6.6 eV for the timescales considered. For an interacting junction as given by the Hamiltonian in Eq. 8, the current is given by (using Eq. 4.114 in (25))

$$I(\eta) = \frac{2e^2V}{h} \left[\frac{\gamma^2}{E_0^2 + (\gamma + \eta)^2} + \frac{\eta\gamma}{E_0^2 + (\gamma + \eta)^2} \right]. \quad (15)$$

The first and second terms represent precisely the first and second contribution in Eq. 3, respectively. However, as we have previously discussed, within this model calculation, the liquid environment is allowed to form coherent interactions with the current-carrying electrons inside the junction. This results in the second term giving rise to orders-of-magnitude increase in the total current to values that are unlikely in the present setting. In the junction, one has to consider also that the bosonic environment scatters the current-carrying electrons in all directions, including along the pore channel where they can be collected into the liquid. This effect is exacerbated by the fact that the environment both carries some longitudinal momentum and can act as a sink for electrons as well, due to the longitudinal bias. Therefore, on physical grounds, we assume that such processes occur which provide only the first contribution to the current in Eq. 3. Again, this is equivalent to assuming a two-probe noise model, as we have discussed previously. Under this assumption and for $\gamma \ll E_0$, the expression in Eq. 15 becomes

$$I(\eta) \approx \frac{2e^2V}{h} \frac{\gamma^2}{E_0^2 + \eta^2}, \quad (16)$$

i.e., the current for just a single structural distortion for linear response and weak coupling, and in the absence of inelastic processes that enhance the current. Note, that irrespective of this approximation, our main conclusions would be qualitatively unchanged.

We know from above that the current acquires a distribution when structural distortions of the DNA are taken into account. Under the assumptions that went into Eq. 14 we can introduce these structural distortions by allowing E_0 or γ to acquire distributions. From Fig. 4, it is clear that the current distributions on a logarithmic scale can be approximated as a Gaussian when no noise is present, which indicates that the coupling to the electrodes is controlling these distributions, as only the coupling fluctuates on an exponential scale. By assuming the coupling to both electrodes is identical, we miss structural distortions which bring the base into closer proximity to one electrode and farther from the other. However, this is unlikely to affect the essential physics.

Now, let us calculate the distribution of γ -values using the curve in Fig. 4 with no noise. Using the fact that the current distribution on a logarithmic scale is approximately a Gaussian, and that we are in a weak coupling regime ($\gamma \ll E_0$), $\ln \gamma/\gamma_m$, where γ_m is the maximum likelihood coupling strength, it should also follow a Gaussian distribution,

$$p(\ln \gamma/\gamma_m) = \frac{1}{\sqrt{2\pi\sigma_\gamma^2}} \exp \left\{ -\frac{(\ln \gamma/\gamma_m)^2}{2\sigma_\gamma^2} \right\}, \quad (17)$$

with the standard deviation $\sigma_\gamma = \sigma_I/2 \approx 0.45$, where σ_I is the standard deviation of $\ln I/I_m$ with $\eta = 0$ and I_m the maximum value. (Note that the relatively small standard deviation of the current distributions $\ln I/I_m$, as seen in Figs. 4 and 5, is a result of the control exerted by the transverse field (18,19). In the absence of such control, the current distributions span several orders of magnitude and have considerable overlap (20).) The maximum, γ_m , appears at 6.8×10^{-4} eV,

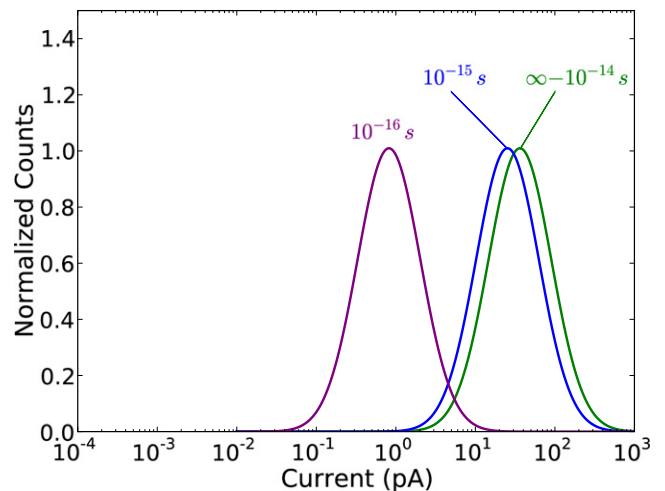


FIGURE 5 Current distributions of a model system for the adenine nucleotide represented by a single energy level E_0 . The current distribution on a logarithmic scale is taken to be Gaussian in similarity to Fig. 4 for no noise. As noise is turned on, at first the distribution does not change at all, but around $\eta \approx E_0$, where $\eta = \hbar/\tau_n$ measures the strength of the noise, the distribution starts to shift. At larger η , the peak of distribution shifts to lower values as η^{-2} . The off-resonant tunneling, indicated by large E_0 as measured from the Fermi level, protects the current distributions from noise.

when $E_0 = 1$ eV—which is approximately the energy separation of Adenine’s LUMO from gold’s Fermi level (1). We assume that the standard deviation of $\ln \gamma/\gamma_m$ does not change when we turn on the noise. The resulting current distributions are plotted in Fig. 5.

Although we assume in our model that the distributions stay Gaussian with the same standard deviation no matter what the noise strength, our model explains the key features found in our numerical simulations. The fact that the molecular energy levels are far away from the electrode Fermi level protects the distributions from this type of noise. This is represented by the term $(E_0^2 + \eta^2)^{-1}$ in the current (Eq. 16). The other features that appear, such as increased broadening and eventual multiple peak development, are not explained by our simple model. These are due to multiple energy levels, E_i , of the fluctuating nucleotide junction, contributing to transport. The contribution from each reaches its turning point, $\eta \approx E_i$, at a different value of η and thus the single peak broadens and develops into multiple peaks.

We now examine the role of transverse bias on the distributions for two different noise strengths (i.e., no noise and a timescale of $\tau_n = 10^{-15}$ s). The results for the cases of 0.1 V and 1.0 V transverse biases are presented in Fig. 6. Previous work has shown that the transverse bias has a nonlinear effect on the mean of the distribution (19). This is due to both a pulling effect of the backbone toward one electrode as the field is increased with consequent alignment of the base toward the other electrode, and the steric effect of the alignment of the backbone with one of the electrodes. Therefore, although one can expect the mean current to be shifted to lower values with lower bias, the degree to which this occurs is not easy to determine a priori. This is especially true with the smaller base T. For this base, one cannot always expect perfect alignment at all times with the electrodes even in the presence of a stabilizing transverse field, further emphasizing the statistical nature of this problem. These effects can be seen in Fig. 6. In addition, one can see that all of the distributions are shifted slightly to lower current values due to noise, corresponding to an overall lowering of the current magnitude. However, the distributions themselves are very similar to the case of an infinite timescale (zero noise).

CONCLUSIONS

In conclusion, we have presented results combining molecular dynamics simulations with quantum mechanical current calculations including a model of noise generated by the complex liquid environment in which the DNA translocation and interrogation takes place. We have shown that for reasonable timescales, e.g., down to 10^{-15} s, the noise considered here will likely not affect the distinguishability of the current distributions obtained from measuring the transverse electronic current of the different DNA nucleotides. At extremely fast timescales, below 10^{-15} s, the distri-

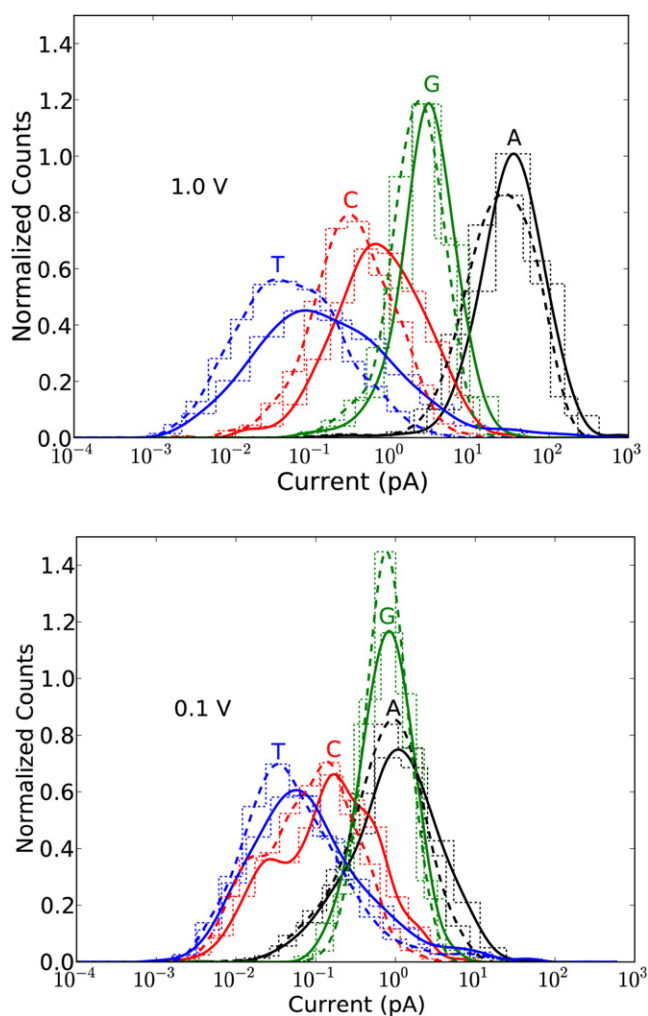


FIGURE 6 Normalized current distributions for the four nucleotides at a transverse bias voltage of 1.0 V (top) and 0.1 V (bottom). The solid lines correspond to an infinite noise timescale (no noise) and the dark dashed lines represent the distributions for $\tau_n = 10^{-15}$ s, with the light dashed lines representing the bins used to produce the distributions.

butions are significantly altered, but this is beyond physically reasonable times for the experimental system we are considering. We have also proposed a simple model system that provides insight into the physical mechanisms of noise and why the current distributions are protected. This is due to the off-resonant nature of tunneling through the nucleotides, and thus it is likely to be a general property of transport in organic molecules. Although the distributions are only mildly affected, we have shown that the type of noise we consider can potentially alter a single current count significantly, further supporting the notion that only a statistical study of the transverse currents can potentially distinguish the nucleotides. We finally note that although our study is done for a nanopore geometry, the results are applicable to other types of sequencing devices as well, such as the nano-channels in the literature (23,24) used in transverse electronic measurements.

SUPPORTING MATERIAL

A movie is available at [http://www.biophysj.org/biophysj/supplemental/S0006-3495\(09\)01282-X](http://www.biophysj.org/biophysj/supplemental/S0006-3495(09)01282-X).

We thank Yonatan Dubi and Johan Lagerqvist for useful discussions.

This research is supported by the National Institutes of Health-National Human Genome Research Institute and by the U.S. Department of Energy through the LANL/LDRD Program.

REFERENCES

- Zwolak, M., and M. Di Ventra. 2008. Physical approaches to DNA sequencing and detection. *Rev. Mod. Phys.* 80:141–165.
- Schloss, J. A. 2008. How to get genomes at one ten-thousandth the cost. *Nat. Biotechnol.* 26:1113–1115.
- Branton, D., D. W. Deamer, A. Marziali, H. Bayley, S. A. Benner, et al. 2008. The potential and challenges of nanopore sequencing. *Nat. Biotechnol.* 26:1146–1153.
- Kasianowicz, J. J., E. Brandin, D. Branton, and D. W. Deamer. 1996. Characterization of individual polynucleotide molecules using a membrane channel. *Proc. Natl. Acad. Sci. USA.* 93:13770–13773.
- Akeson, M., D. Branton, J. Kasianowicz, E. Brandin, and D. Deamer. 1999. Microsecond time-scale discrimination among polycytidylic acid, polyadenylic acid, and polyuridylic acid as homopolymers or as segments within single RNA molecules. *Biophys. J.* 77:3227–3233.
- Meller, A., L. Nivon, E. Brandin, J. Golovchenko, and D. Branton. 2000. Rapid nanopore discrimination between single polynucleotide molecules. *Proc. Natl. Acad. Sci. USA.* 97:1079–1084.
- Meller, A., L. Nivon, and D. Branton. 2001. Voltage-driven DNA translocations through a nanopore. *Phys. Rev. Lett.* 86:3435–3438.
- Mathe, J., A. Aksimentiev, D. Nelson, K. Schulten, and A. Meller. 2005. Orientation discrimination of single-stranded DNA inside the α -hemolysin membrane channel. *Proc. Natl. Acad. Sci. USA.* 102:12377–12382.
- Butler, T., J. Gundlach, and M. Troll. 2006. Determination of RNA orientation during translocation through a biological nanopore. *Biophys. J.* 90:190–199.
- Astier, Y., O. Braha, and H. Bayley. 2006. Toward single molecule DNA sequencing: direct identification of ribonucleoside and deoxyribonucleoside 5'-monophosphates by using an engineered protein nanopore equipped with a molecular adapter. *J. Am. Chem. Soc.* 128:1705–1710.
- Li, J., M. Gershow, D. Stein, E. Brandin, and J. Golovchenko. 2003. DNA molecules and configurations in a solid-state nanopore microscope. *Nat. Mater.* 2:611–615.
- Chen, P., J. Gu, E. Brandin, Y. Kim, Q. Wang, et al. 2004. Probing single DNA molecule transport using fabricated nanopores. *Nano Lett.* 4:2293–2298.
- Storm, A., C. Storm, J. Chen, H. Zandbergen, J.-F. Joanny, et al. 2005. Fast DNA translocation through a solid-state nanopore. *Nano Lett.* 5:1193–1197.
- Fologea, D., M. Gershow, B. Ledden, D. McNabb, J. Golovchenko, et al. 2005. Detecting single stranded DNA with a solid state nanopore. *Nano Lett.* 5:1905–1909.
- Chang, H., F. Kosari, G. Andreadakis, M. Alam, G. Vasmatzis, et al. 2004. DNA-mediated fluctuations in ionic current through silicon oxide nanopore channels. *Nano Lett.* 4:1551–1556.
- Heng, J., C. Ho, T. Kim, R. Timp, A. Aksimentiev, et al. 2004. Sizing DNA using a nanometer-diameter pore. *Biophys. J.* 87:2905–2911.
- Zwolak, M., and M. Di Ventra. 2005. Electronic signature of DNA nucleotides via transverse transport. *Nano Lett.* 5:421–424.
- Lagerqvist, J., M. Zwolak, and M. Di Ventra. 2006. Fast DNA sequencing via transverse electronic transport. *Nano Lett.* 6:779–782.
- Lagerqvist, J., M. Zwolak, and M. Di Ventra. 2007. Influence of the environment and probes on rapid DNA Sequencing via transverse electronic transport. *Biophys. J.* 93:2384–2390.
- Lagerqvist, J., M. Zwolak, and M. Di Ventra. 2007. Comment on characterization of the tunneling conductance across DNA bases. *Phys. Rev. E Stat. Nonlin. Soft Matter Phys.* 76:013901.
- Gierhart, B. C., D. G. Howitt, S. J. Chen, Z. Zhu, D. E. Kotecki, et al. 2008. Nanopore with transverse nanoelectrodes for electrical characterization and sequencing of DNA. *Sens. Actuators B Chem.* 132:593–600.
- Fischbein, M. D., and M. Drndić. 2007. Sub-10 nm device fabrication in a transmission electron microscope. *Nano Lett.* 7:1329–1337.
- Liang, X., and S. Y. Chou. 2008. Nanogap detector inside nanofluidic channel for fast real-time label-free DNA analysis. *Nano Lett.* 8:1472–1476.
- Maleki, T., S. Mohammadi, and B. Ziaie. 2009. A nanofluidic channel with embedded transverse nanoelectrodes. *Nanotechnology.* 20:105302.
- Di Ventra, M. 2008. *Electrical Transport in Nanoscale Systems*. Cambridge University Press, Cambridge, UK.
- Zwolak, M., and M. Di Ventra. 2004. DNA electronics. In *Encyclopedia of Nanoscience and Nanotechnology*, Vol. 2. H. S. Nalwa, editor. American Scientific Publishers, Stevenson Ranch, CA.
- Endres, R., D. Cox, and R. Singh. 2004. The quest for high-conductance DNA. *Rev. Mod. Phys.* 76:195–214.
- Shapir, E., H. Cohen, A. Calzolari, C. Cavazzoni, D. A. Ryndyk, et al. 2008. Electronic structure of single DNA molecules resolved by transverse scanning tunneling spectroscopy. *Nat. Mater.* 7:68–74.
- Phillips, J. C., R. Braun, W. Wand, J. Gumbart, E. Tajkhorshid, et al. 2005. Scalable molecular dynamics with NAMD. *J. Comput. Chem.* 26:1781–1802.
- Foloppe, N., J. Alexander, and D. Mackerell. 2000. All-atom empirical force field for nucleic acids. I. Parameter optimization based on small molecule and condensed phase macromolecular target data. *J. Comput. Chem.* 21:86–104.
- Alexander, D., J. Mackerell, and N. K. Banavali. 2000. All-atom empirical force field for nucleic acids. II. Application to molecular dynamics simulations of DNA and RNA in solution. *J. Comput. Chem.* 21:105–120.
- Wendel, J. A., and W. A. Goddard III. 1992. The Hessian biased force field for silicon nitride ceramics: predictions of thermodynamic and mechanical properties for α - and β -Si₃N₄. *J. Chem. Phys.* 97:5048–5062.
- Aksimentiev, A., J. B. Heng, G. Timp, and K. Schulten. 2004. Microscopic kinetics of DNA translocation through synthetic nanopores. *Biophys. J.* 87:2086–2097.
- Macke, T., and D. Case. 1997. Modeling unusual nucleic acid structures. In *Molecular Modeling of Nucleic Acids*. N. B. Leontis and J. SantaLucia, editors. American Chemical Society, Washington, DC.
- Pecchia, A., M. Gheorghe, A. Di Carlo, P. Lugli, T. Niehaus, et al. 2003. Role of thermal vibrations in molecular wire conduction. *Phys. Rev. B.* 68:235321.
- Büttiker, M. 1986. 4-Terminal phase-coherent conductance. *Phys. Rev. Lett.* 57:1761–1764.
- Chen, Y., M. Zwolak, and M. Di Ventra. 2003. Local heating in nanoscale conductors. *Nano Lett.* 3:1691–1694.
- Chen, Y., M. Zwolak, and M. Di Ventra. 2004. Inelastic current-voltage characteristics of atomic and molecular junctions. *Nano Lett.* 4:1709–1712.
- Zwolak, M., and M. Di Ventra. 2002. DNA spintronics. *Appl. Phys. Lett.* 81:925–927.
- Jauho, A., N. Wingreen, and Y. Meir. 1994. Time-dependent transport in interacting and noninteracting resonant-tunneling systems. *Phys. Rev. B.* 50:5528–5544.
- Mahan, G. D. 2007. *Many Particle Physics*. Springer, New York.
- Garg, A., J. Onuchic, and V. Ambegaokar. 1985. Effect of friction on electron transfer in biomolecules. *J. Chem. Phys.* 83:4491.
- Humphrey, W., A. Dalke, and K. Schulten. 1996. VMD—visual molecular dynamics. *J. Mol. Graph.* 14:33–38.